A shear warping kinematic enhancement for fiber beam elements with a damaging cross-section

Sophie Capdevielle, Stéphane Grange, Frédéric Dufour, Cédric Desprez

A shear warping kinematic enhancement for fiber beam elements with a damaging cross-section

Capdevielle Sophie[a,b,1], Grange Stéphane[c], Dufour Frédéric[d], Desprez Cédric[e]

[a]*LMT, ENS Cachan, CNRS, Université Paris-Saclay, 94235 Cachan, France*
[b]*Univ. Grenoble Alpes, CNRS, Grenoble INP, 3SR, F-38000 Grenoble, France*
sophie.capdevielle@univ-grenoble-alpes.fr

[c]*Univ. Lyon, INSA-Lyon, GEOMAS, F-69621 Villeurbanne, France*
stephane.grange@insa-lyon.fr

[d]*Univ. Grenoble Alpes, CNRS, Grenoble INP * , 3SR, F-38000 Grenoble, France*
frederic.dufour@3sr-grenoble.fr

[e]*MAST-EMGCU, Univ. Gustave Eiffel, IFSTTAR, F-77447 Marne-la-Vallée, France*
cedric.desprez@univ-eiffel.fr

Abstract

The present paper is dedicated to the modeling of the non-linear behavior of reinforced concrete structures subject to transverse shear or torsion under monotonic and cyclic loading. The fiber beam element approach has been proved to be an interesting modeling strategy, but needs to be improved for shear effects. This can be achieved by enhancing the cross-section kinematics with a warping displacement field. This field must be free from the cross-section rigid body motions, for the problem to be well posed. This condition can be enforced by projecting the warping displacements orthogonally to the space of the plane cross-section displacements. The present contribution proposes a kinematic enhancement for a Timoshenko fiber beam element with a new formulation of the projection functions. The warping shape of the cross-section is computed along with the beam displacements and rotations by an implicit solution procedure. The proposed formulation takes into account the possible material heterogeneity of the cross-section. It enables the warping

---

[1]Corresponding author
[*]Institute of Engineering and Management, Univ. Grenoble Alpes

profile to evolve in time with the material damage state, as may occur in reinforced concrete structures. The element formulation is validated using an analytical solution in the case of transverse shear, and 3D simulations of beams subject to shear and torsion. To address nonlinear behavior, a comparison to experimental results is performed. The first case study shows that including warping in the model drastically improves the prediction of the experimental behavior of concrete beams in torsion. The second case study shows the ability of the model to deal with cyclic bending of a reinforced concrete column.

1. Introduction

The evaluation of the vulnerability of existing structures is one of the current challenges in Civil Engineering. In order to check the structural safety of reinforced concrete structures, accurate, robust, and efficient numerical methods must be used. These methods must handle several materials, which state may evolve during the loading due to damage and plasticity. Furthermore, to assess the seismic vulnerability of structures, the cyclic behavior of these materials must be well-represented. The finite element method based on continuum mechanics is by far the most popular approach for computations at the structural scale. However, one can benefit from the slenderness of some structural elements and use the beam theory to drastically reduce the computational time. The fiber beam element method has been proved to lead to accurate results when modeling existing reinforced concrete structures [1, 2], with a reasonably low computational cost. Based on beam elements, fiber beam elements consist in adding a scale to the model by considering the strains and stresses at the cross-section level [3]. The principle of displacement-based fiber beam elements is explained in figure 1. As in the beam element method, generalized strains $\mathbf{e}_s$ are computed at the integration point of the element from the displacements and rotations $\mathbf{U}$ at the nodes. However, fiber elements do not use a constitutive direct equation between generalized strains and internal forces. The actual strains $\boldsymbol{\epsilon}$ are computed at the cross-section level, based on a kinematic assumption for the cross-section behavior. The stresses $\boldsymbol{\sigma}$ are computed from the strains according to the chosen constitutive laws. The generalized forces $\boldsymbol{F}$ are eventually computed
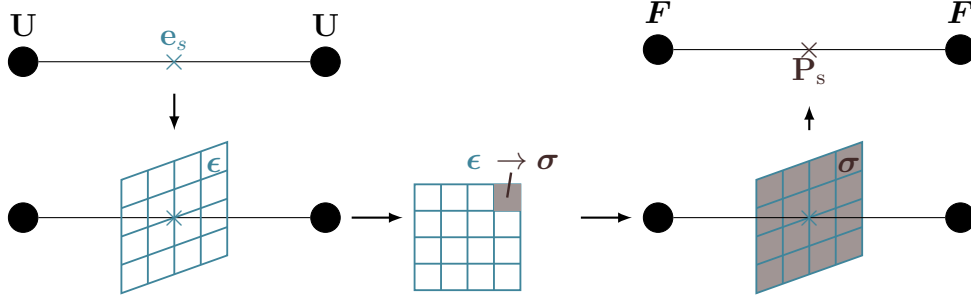
by stress integration over the cross-section.

Figure 1: The fiber beam element: a multiscale approach

By replacing the generalized constitutive law at the cross-section scale, the fiber beam element method is particularly suitable for computing the structural behavior. Indeed, it enables to access precise information at the material scale, like the level of material damage. Yet, if the method has proved to be efficient to model slender frame structures mainly subject to normal stresses, it fails to deal with structures subject to higher shear stresses or torsion. As an example, Mazars et al. [4] related how multilayered beam elements, which are the 2D version of fiber beam elements, managed to predict the seismic behavior of walls with a slenderness of 0.7, while failing to predict the behavior of walls with a slenderness of 0.4. Indeed, the computation of the cross-section strains is based on the plane cross-section kinematics. When subject to large shear stresses, the cross-section does not remain plane, but warps. The warping deformations have to be added in the fiber element computation of strains to enable accurate modeling of shear behavior.

To address this issue, several authors have built enhanced fiber elements. Vecchio and Collins [5] proposed to satisfy the local multilayered section equilibrium with a homogenized concrete behavior to accurately compute shear stresses. Efficient and accurate under monotonic loading, the model is limited when dealing with cyclic loading. Dubé [6] proposed to enhance a multilayered beam element by adding transverse shear warping. The warping shape of the cross-section is computed by satisfying the elastic equilibrium between the cross-section layers. The warping shape of the cross-section is then kept constant during the computation, and thus does not account for damage evolution. The same concept of fixed strain pattern is behind the

model of Mazars et al. [7], who enhanced a beam element by adding a torsion warping profile, computed by the local equilibrium of the cross-section. The drawback of the fixed warping pattern is the unability of the model to account for the effect of damage and cracking on warping. Based on [7], Capdevielle et al. [8] developed an enhanced beam element with torsional warping updated with the evolution of the material damage. Though, this element ignored transverse shear warping. In addition to that, the warping shape was computed based on the material properties of the previous converged time step, which introduced a small load step dependency of the results.

Further enhancements accounting for evolving warping profiles have been presented in [9, 10, 11, 12]. Bairan and Mari [9, 10, 11] proposed an enhanced cross-section model, by adding warping and distorsion displacements to the displacement field of the plane cross-section. Mohr et al. [12] implemented the cross-section model in a 2D displacement-based Bernoulli fiber beam element. More recently, Poliotti and Bairán [13] have proposed a new version of this model by using spline functions for the interpolation of the warping displacements. The model exhibits good results in transverse shear. However, the additional displacements do not vary in the longitudinal direction, which constrains the resolution. Namely, the variational formulation contains the derivative of the axial stress, that needs to be approximated during the solution procedure [10]. Thus stresses and warping are not fully coupled and the solution procedure cannot be completely implicit.

On the other hand, a fully implicit approach is used by Le Corvec [14]. A mixed-formulated fiber beam element is enhanced by adding warping varying in both the transverse and longitudinal directions to the cross-section displacements. This approach is very efficient to model the behavior of structural elements subject to shear, with an elasto-plastic material. Di Re et al. [15] have added the inertia effects to the model, to represent the dynamic vibration of thin-walled structures in torsion. Another enhancement of force-based elements to account for warping in elasto-plastic frames has been proposed by Almeida et al. [16]. The advantage of force-based or mixed-based formulations is the small number of beam elements required to obtain an accurate solution. The exact deformed shape in linear elasticity is obtained with only one element, and dealing with nonlinearities requires only few beam elements. However, an additional internal loop is needed for the element state determination. This requires the section stiffness to be well-conditioned, which is the case for an elasto-plastic material with kinematic

4

hardening. Perfect plasticity or softening however require specific numerical strategies [17], for which an enhancement of the element would not be a straightforward step. Addessi and Di Re [18] have coupled the enhancement proposed by Le Corvec [14] with a damaging material for applications in torsion, by linearizing the constitutive equations in the element state determination algorithm. Although it is an interesting approach, damage related to the cyclic response of concrete structural elements, or to warping due to transverse shear have not been investigated with mixed-formulated beam elements, to the authors' knowledge.

The present contribution proposes a formulation based on the models of Bairan and Mari [10] and Le Corvec [14], with a new proposition for the warping shape function projection. A displacement-based approach is chosen, to avoid dealing with the cross-section singularities inherent to force-based beam elements. A finite element cross-section discretization is used here, to enable a fine representation of damage evolution in the cross-section. The novelty of the approach proposed here is the coupled evolution of warping and damage computed with a fully-implicit solution procedure based on the beam equilibrium only. It can be used for the computation of non-linear concrete structures under transverse shear and/or torsion, and is able to deal with a cyclic loading.

The governing equations of the enhanced displacement-based fiber element are presented in a first part. A validation of the formulation is then proposed, by comparing the results on a beam with a linear elastic behavior to a reference solution. In the case of transverse shear, the computed strains are compared to the analytical solution. In the case of combined flexure and torsion, the results are compared to a 3D computation. The formulation is then confronted with experimental results. The case of concrete beams subject to monotonic torsion is investigated, followed by the case of reinforced concrete columns subject to reverse cyclic bending.

2. Governing equations of the enhanced element

2.1. Warping kinematics

A 3D displacement-based fiber beam element is enhanced by adding warping displacements. Total displacements in the beam are given by equation (1). $\mathbf{u}^p$ contains the displacements of the plane cross-section, according to Timoshenko's beam theory. u, v and w are the mean displacements and

θ_x, θ_y, θ_z the mean rotations of the beam's cross section. $\mathbf{u}^w$ is the additional warping displacement vector. These out-of-plane displacements can obviously vary in the transverse directions y and z. They are also allowed to vary in the longitudinal x direction, which enables the formulation to account for restrained warping boundary conditions and different damage states along the beam.

$$\mathbf{u} = \mathbf{u}^p + \mathbf{u}^w = \begin{bmatrix} u - y\,\theta_z + z\,\theta_y \\ v - z\,\theta_x \\ w + y\,\theta_x \end{bmatrix} + \begin{bmatrix} u_x^w(x,y,z) \\ 0 \\ 0 \end{bmatrix} \tag{1}$$

The linearized strain tensor accounting for warping is given by equation (2). For the beam element formulation, this tensor is expressed as a strain vector $\boldsymbol{\epsilon}$, given by equation (3). From the kinematic enhancement, a term corresponding to the warping strains $\boldsymbol{\varepsilon}^w$ adds to the plane cross-section strains $\boldsymbol{\varepsilon}^p$.

$$\varepsilon = \frac{1}{2}\left(\mathbf{grad}(\mathbf{u}) + \mathbf{grad}(\mathbf{u})^T\right) = \boldsymbol{\varepsilon}^p + \boldsymbol{\varepsilon}^w \tag{2}$$

$$\boldsymbol{\epsilon} = \begin{bmatrix} \epsilon_{xx} \\ 2\epsilon_{xy} \\ 2\epsilon_{xz} \end{bmatrix} = \underbrace{\begin{bmatrix} \frac{du}{dx} - y\frac{d\theta_z}{dx} + z\frac{d\theta_y}{dx} \\ -z\frac{d\theta_x}{dx} + \frac{dv}{dx} - \theta_z \\ y\frac{d\theta_x}{dx} + \frac{dw}{dx} + \theta_y \end{bmatrix}}_{\boldsymbol{\epsilon}^p} + \underbrace{\begin{bmatrix} \frac{\partial u_x^w}{\partial x} \\ \frac{\partial u_x^w}{\partial y} \\ \frac{\partial u_x^w}{\partial z} \end{bmatrix}}_{\boldsymbol{\epsilon}^w} \tag{3}$$

2.2. Equilibrium equation and variational formulation

Assuming that there is no body force, the beam equilibrium equation reads:

$$\mathrm{div}\left(\boldsymbol{\sigma}\right) = 0 \tag{4}$$

The Cauchy's stress tensor $\boldsymbol{\sigma}$ depends on the displacements through a non linear material relationship relating stresses and strains : $\boldsymbol{\sigma} = \hat{\boldsymbol{\sigma}}\left(\boldsymbol{\varepsilon}^p, \boldsymbol{\varepsilon}^w\right)$. Let $\mathcal{D}$ denote the trial solution space and Δ the variation space. With Ω denoting the beam domain, the variational form of the equilibrium equation (4) is given by:

$$\begin{cases} \text{Find } \mathbf{u} \in \mathcal{D}, \text{ such that } \forall\, \delta\mathbf{u} \in \Delta, \\ \qquad \int_\Omega \delta\mathbf{u}^T \mathrm{div}\left(\boldsymbol{\sigma}\right) d\Omega = 0 \end{cases} \tag{5}$$

With $\mathcal{D}^p$ and Δ^p the trial and variation spaces for the plane section displacements $\mathbf{u}^p$, and $\mathcal{D}^w$ and Δ^w the trial and variation spaces for the warping displacements, equation (5) can be rewritten as:

$$\begin{cases} \text{Find } \mathbf{u}^p \in \mathcal{D}^p \text{ and } \mathbf{u}^w \in \mathcal{D}^w, \text{ such that } \forall \, \delta\mathbf{u}^p \in \Delta^p \text{ and } \forall \, \delta\mathbf{u}^w \in \Delta^w, \\ \qquad \int_\Omega \left(\delta\mathbf{u}^{pT} + \delta\mathbf{u}^{wT} \right) \operatorname{div}(\boldsymbol{\sigma}) \, d\Omega = 0 \end{cases} \tag{6}$$

With no further requirements on the solution displacements $\mathbf{u}^p$ and $\mathbf{u}^w$, the problem is ill-posed. The solution is not unique, because no condition prevents $\mathbf{u}^w$ from containing a plane displacement solution. To address this problem, the warping displacements $\mathbf{u}^w$ are required to be orthogonal to the plane displacements $\mathbf{u}^p$. The consequences of this requirement on the implementation are exposed in section 2.4. With this orthogonality requirement, the weak form of the equilibrium equation can be projected on Δ^p and Δ^w. The variational form of the equilibrium equations thus reads:

Find $\mathbf{u}^p \in \mathcal{D}^p$ and $\mathbf{u}^w \in \mathcal{D}^w$, such that:

$$\forall \, \delta\mathbf{u}^p \in \Delta^p, \quad \int_\Omega \delta\mathbf{u}^{pT} \operatorname{div}(\boldsymbol{\sigma}) \, d\Omega = 0 \tag{7}$$

$$\forall \, \delta\mathbf{u}^w \in \Delta^w, \quad \int_\Omega \delta\mathbf{u}^{wT} \operatorname{div}(\boldsymbol{\sigma}) \, d\Omega = 0 \tag{8}$$

Equation (7) reflects the global beam equilibrium, as shown by Bairan and Mari [10]. Equation (8) reflects the local beam equilibrium in the cross-section, which is not considered in classical fiber beam elements. This local equilibrium equation ensures the transverse inter-fiber equilibrium. After integrating by parts equations (7) and (8), the final variational form of the equilibrium equations (9) and (10) is obtained. $\mathbf{n}$ is the outward unit normal vector to the beam boundaries $\partial\Omega$.

$$\int_\Omega \delta\boldsymbol{\epsilon}^{pT} \boldsymbol{\sigma} \, d\Omega = \int_{\partial\Omega} \delta\mathbf{u}^{pT} \left(\boldsymbol{\sigma}\mathbf{n} \right) dS \tag{9}$$

$$\int_\Omega \delta\boldsymbol{\epsilon}^{wT} \boldsymbol{\sigma} \, d\Omega = \int_{\partial\Omega} \delta\mathbf{u}^{wT}_x \left(\sigma_{xx} n_x \right) dS \tag{10}$$

The right-hand side of equation (10) accounts for the forces due to constrained warping. If the beam is free to warp, equation (10) becomes:

$$\int_\Omega \delta \boldsymbol{\epsilon}^{wT} \boldsymbol{\sigma} \ d\Omega = 0 \qquad (11)$$

2.3. Discretization of the equilibrium equations

The formulation of the enhanced beam element follows the finite element process [19], applied to fiber beam elements. Equations (9) and (10) are spatially discretized to get the element and section matrices. The deformations are discretized first. From equation (3), the plane section strain vector is written in equation (12) in terms of a transformation matrix $\mathbf{a}_s$ and the section generalized strains $\mathbf{e}_s$.

$$\boldsymbol{\epsilon}^p = \begin{bmatrix} 1 & 0 & 0 & 0 & z & -y \\ 0 & 1 & 0 & -z & 0 & 0 \\ 0 & 0 & 1 & y & 0 & 0 \end{bmatrix} \begin{bmatrix} \frac{du}{dx} \\ \frac{dv}{dx} - \theta_z \\ \frac{dw}{dx} + \theta_y \\ \frac{d\theta_x}{dx} \\ \frac{d\theta_y}{dx} \\ \frac{d\theta_z}{dx} \end{bmatrix} = \mathbf{a}_s(y, z) \, \mathbf{e}_s(x) \qquad (12)$$

A separate interpolation method for the longitudinal and transverse directions is assumed for the warping displacement to adapt to the beam discretization (equation (13)). Consequently, the warping strain vector is expressed in equation (14).

$$u_x^w(x, y, z) = c(x) \, \varphi(y, z) \qquad (13)$$

$$\boldsymbol{\epsilon}^w = \begin{bmatrix} \frac{dc}{dx} \varphi \\ c \frac{\partial \varphi}{\partial y} \\ c \frac{\partial \varphi}{\partial z} \end{bmatrix} = \begin{bmatrix} \varphi & 0 \\ 0 & \frac{\partial \varphi}{\partial y} \\ 0 & \frac{\partial \varphi}{\partial z} \end{bmatrix} \begin{bmatrix} \frac{dc}{dx} \\ c \end{bmatrix} = \bar{\mathbf{a}}_w(y, z) \, \mathbf{e}_w(x) \qquad (14)$$

The considered structure is discretized into n_{el} fiber beam elements. The element degrees of freedom are collected into the vectors $\mathbf{U}_{el}^p$ and $\mathbf{U}_{el}^w$. $\mathbf{U}_{el}^p$ contains the classical nodal displacements and rotations. $\mathbf{U}_{el}^w$ contains the warping degrees of freedom at the beam element nodes. The degrees of freedom are interpolated over the beam elements through the use of shape functions and their derivatives, contained in the matrices $\boldsymbol{B}_p$ and $\boldsymbol{B}_w$. The matrices $\mathbf{a}_s$ and $\bar{\mathbf{a}}_w$ contain the shape functions over the cross-section. With

8

these notations, the strain vector's plane and warping parts can be rewritten as:

$$\boldsymbol{\epsilon}^p = \mathbf{a}_s \mathbf{e}_s = \mathbf{a}_s \boldsymbol{B}_p \mathbf{U}_{el}^p \tag{15}$$

$$\boldsymbol{\epsilon}^w = \bar{\mathbf{a}}_w \mathbf{e}_w = \bar{\mathbf{a}}_w \boldsymbol{B}_w \mathbf{U}_{el}^w \tag{16}$$

The expressions of $\boldsymbol{\epsilon}^p$ and $\boldsymbol{\epsilon}^w$ are introduced into the variational form of the equilibrium equations given by equations (9) and (10). The symbol $\hat{\boldsymbol{\sigma}}$ is used to differentiate the constitutive law from the stress tensor ins its matrix form. With $\boldsymbol{\mathcal{U}}^*$ and $\boldsymbol{\mathcal{W}}^*$ denoting the vectors obtained by assembly of the virtual plane and warping displacements respectively, equations (9) and (10) respectively become :

$$\boldsymbol{\mathcal{U}}^{*T} \overset{n_{el}}{\underset{e=1}{\mathbf{A}}} \int_{\Omega^e} \boldsymbol{B}_p^T \mathbf{a}_s{}^T \hat{\boldsymbol{\sigma}} \left(\boldsymbol{\epsilon}^p, \boldsymbol{\epsilon}^w \right) \ d\Omega^e = \boldsymbol{\mathcal{U}}^{*T} \overset{n_{el}}{\underset{e=1}{\mathbf{A}}} \boldsymbol{F}_{\text{ext}}^e \tag{17}$$

$$\boldsymbol{\mathcal{W}}^{*T} \overset{n_{el}}{\underset{e=1}{\mathbf{A}}} \int_{\Omega^e} \boldsymbol{B}_w^T \mathbf{a}_w{}^T \hat{\boldsymbol{\sigma}} \left(\boldsymbol{\epsilon}^p, \boldsymbol{\epsilon}^w \right) \ d\Omega^e = \boldsymbol{\mathcal{W}}^{*T} \overset{n_{el}}{\underset{e=1}{\mathbf{A}}} \boldsymbol{F}^{we} \tag{18}$$

Equations (17) and (18) lead to the set of non-linear equations to be solved for the structure (19). $\boldsymbol{F}_{\text{ext}}$ are the external forces applied to the structure nodes, and $\boldsymbol{F}^w$ are internal efforts due to restrained warping. This is how the element internal force vector $\mathbf{P}_{el}$ is derived.

$$\overset{n_{el}}{\underset{e=1}{\mathbf{A}}} \underbrace{\begin{bmatrix} \int_{\Omega^e} \boldsymbol{B}_p^T \mathbf{a}_s{}^T \hat{\boldsymbol{\sigma}} \left(\boldsymbol{\epsilon}^p, \boldsymbol{\epsilon}^w \right) \ d\Omega^e \\ \int_{\Omega^e} \boldsymbol{B}_w^T \mathbf{a}_w{}^T \hat{\boldsymbol{\sigma}} \left(\boldsymbol{\epsilon}^p, \boldsymbol{\epsilon}^w \right) \ d\Omega^e \end{bmatrix}}_{\mathbf{P}_{el}} = \begin{bmatrix} \boldsymbol{F}_{\text{ext}} \\ \boldsymbol{F}^w \end{bmatrix} \tag{19}$$

2.4. Enforcement of the orthogonality requirement

As mentioned in section 2.2, warping displacements have to be orthogonal to the plane section displacements to allow a unique solution. This requirement needs to be enforced in the formulation. Le Corvec [14] proposed a projection for the transverse shape functions used to compute the warping

displacements. The shape functions are projected to a space orthogonal to the plane displacement solution. However, the deformations are not computed using the derivatives of the shape functions. To address this issue, the present paper proposes a projection method, which computes the derivatives of the projected shape functions.

The enhancement consists of the warping displacement in the longitudinal direction only (equation (1)). As can be seen in equation (1), the axial component of the Timoshenko's displacement u_x^p is generated by the base functions 1, y and z. From the original interpolation functions over the cross section $\boldsymbol{N}_i$, the projected shape functions $\tilde{\boldsymbol{N}}_i$ are given by equations (20) and (21). $\mathcal{S}$ represents the cross-section domain. The shape functions derivatives are computed in equation (22).

$$\tilde{\boldsymbol{N}}_i = \boldsymbol{N}_i - \int_{\mathcal{S}} \boldsymbol{N}_i \begin{bmatrix} \frac{1}{a_1} & \frac{y}{a_2} & \frac{z}{a_3} \end{bmatrix} d\mathcal{S} \begin{bmatrix} 1 \\ y \\ z \end{bmatrix} \tag{20}$$

$$\text{Where} \quad a_1 = \int_{\mathcal{S}} 1 \, d\mathcal{S} \quad ; \quad a_2 = \int_{\mathcal{S}} y^2 \, d\mathcal{S} \quad ; \quad a_3 = \int_{\mathcal{S}} z^2 \, d\mathcal{S} \tag{21}$$

$$\frac{\partial \tilde{\boldsymbol{N}}_i}{\partial y} = \frac{\partial \boldsymbol{N}_i}{\partial y} - \int_{\mathcal{S}} \boldsymbol{N}_i \frac{y}{a_2} d\mathcal{S} \qquad \text{and} \qquad \frac{\partial \tilde{\boldsymbol{N}}_i}{\partial z} = \frac{\partial \boldsymbol{N}_i}{\partial z} - \int_{\mathcal{S}} \boldsymbol{N}_i \frac{z}{a_3} d\mathcal{S} \tag{22}$$

Theoretically, the formulation proposed in [14] leads to the same expressions for $\frac{\partial \tilde{\boldsymbol{N}}_i}{\partial y}$ and $\frac{\partial \tilde{\boldsymbol{N}}_i}{\partial z}$, only if the transverse shape functions satisfy the conditions (23). n_w is the number of warping degrees of freedom, and (y_i, z_i) the coordinates of the corresponding warping nodes. Conditions (23) seem to be verified for Lagrange polynomials. However, they are not true in the general case, to the authors' knowledge.

$$\begin{cases} \sum_{i=1}^{n_w} \frac{\partial \boldsymbol{N}_i}{\partial y} = 0 \; ; \quad \sum_{i=1}^{n_w} \frac{\partial \boldsymbol{N}_i}{\partial z} = 0 \\ \sum_{i=1}^{n_w} \frac{\partial \boldsymbol{N}_i}{\partial y} y_i = 1 \; ; \quad \sum_{i=1}^{n_w} \frac{\partial \boldsymbol{N}_i}{\partial y} z_i = 0 \\ \sum_{i=1}^{n_w} \frac{\partial \boldsymbol{N}_i}{\partial z} y_i = 0 \; ; \quad \sum_{i=1}^{n_w} \frac{\partial \boldsymbol{N}_i}{\partial z} z_i = 1 \end{cases} \tag{23}$$

a_1, a_2 and a_3 (equation (21)) are computed by numerical integration over

the cross-section. The precision of the computation of a_1, a_2 and a_3 is crucial for the projection's accuracy. The choice for the cross-section discretization is explained in section 2.5.

2.5. Spatial discretization of the cross-section and interpolation functions

When dealing with damaging concrete, accurate modeling of the spatial distribution of damage along the cross-section is needed. This automatically leads to an increase of the number of interpolation points in the cross-section. Le Corvec [14] and Addessi and Di Re [18] have proposed applications with warping degrees of freedom interpolated using 2D Lagrange polynomials. Even if this is an efficient interpolation strategy, it limits the number of interpolation points that can be used in the cross-section. Indeed, increasing the number of polynomials leads to spurious oscillations between the interpolation points, known as Runge's phenomenon. If the number of interpolation points is limited, the spatial variability of damage is necessarily averaged. For these reasons, a finite element element modeling strategy has been chosen for the cross-section here.

Another possible solution to avoid this drawback of the Lagrange polynomials is to use spline functions [13]. However, numerous integration points would still be needed to deal with the variation of the damage state of the material over the cross-section. In addition to this, when the section damages, especially in torsion, its warping profile becomes sharper. Capturing this shape with accuracy would require to increase the number of interpolating functions, and thus the number of interpolating points.

The cross-section is thus discretized here in 2D finite elements, which can be as numerous as needed, to take into account the local variation of the material state. Three integration points by element are needed for the exact computation of the integrals of quadratic functions for the computation of a_2 and a_3. This is necessary for the exact computation of the rigid body motions of the cross-section to get a warping displacement free from the section global rotations. The cross-section is thus discretized by quadratic 6-nodes triangles.

The presented enhancement has been implemented in a linear displacement-based Timoshenko fiber beam element. The numerical examples presented in the following parts are computed with the presented element, implemented in the **ATL4S** [20] finite element code.

11

3. Validation of the linear behavior at the cross-section scale

In this section, the warping profile in a beam modeled with the enhanced element is computed. The case of transverse shear and combined shear and torsion loading are studied successively. For each type of loading, a cantilever beam of of length $1\,\mathrm{m}$ with a rectangular cross-section with dimensions $0.1\,\mathrm{m} \times 0.2\,\mathrm{m}$ is tested. A linear elastic constitutive law is used for the material behavior. The numerical examples presented here aim at validating the formulation and the implementation for simple cases.

3.1. Warping due to transverse shear

This part is dedicated to the formulation validation for the case of transverse shear. The beam is subjected to a transverse load of $1\,\mathrm{kN}$ at its free end. The beam is discretized using 10 enhanced fiber beam elements. A relatively high number of beam elements is chosen here to avoid the classical displacement error due to the use of linear shape functions in the longitudinal direction. The cross-section is discretized using 6-node quadratic triangles, as explained in part 2.5. A regular mesh of 64 triangular elements is used. This relatively high number of elements in the cross-section would actually not be necessary for a linear-elastic case-study. It is the mesh used in section 4 for computations with a damaging material, when it is interesting to have precise values of damage in the transverse directions of the beam. The case-study's geometry is displayed in figure 2. The material linear elastic features are set to $E = 30\,\mathrm{GPa}$ and $\nu = 0.2$.
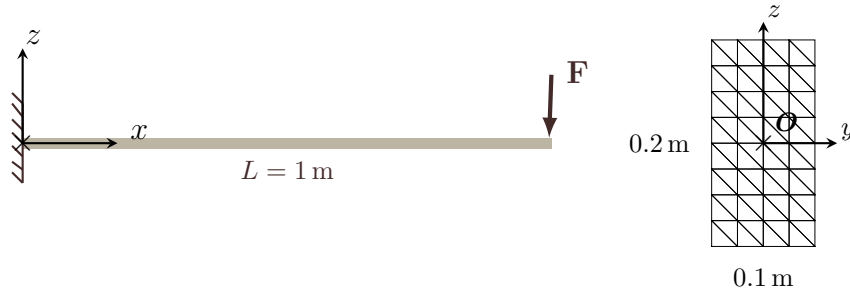

Figure 2: Case study used for the analytical validation of the enhanced fiber beam element: beam geometry and loading; and cross-section mesh.

Figure 3(a) displays the computed warping displacements in the cross-section. The studied beam is loaded only in the z direction. Accordingly, warping displacements are constant in the y direction.

According to Jourawsky's theory, the analytical expression for the shear strains ϵ_{xz} in the cross-section is given by equation (24).

$$\epsilon_{xz}\left(x, z\right) = \frac{V_z}{2GI_y}\left((h/2)^2 - z^2\right) \tag{24}$$
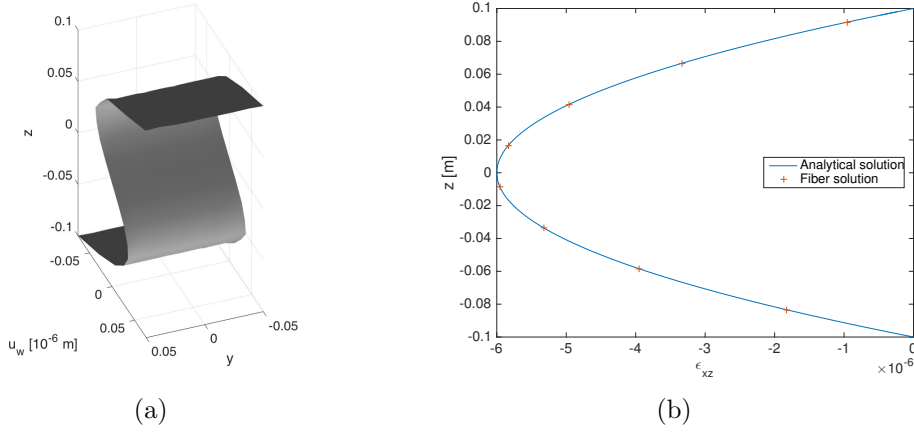

(a)　　　　　　　　　　(b)

Figure 3: Results for the bended cantilever beam case-study. 3(a): Warping displacements of the rectangular cross-section under shear. 3(b): Comparison of the computed shear strains to the analytical shear strains for the bended cantilever beam.

The numerical strains are computed in each Gauss point of the cross-section. The strains ϵ_{xz} do not vary in the y direction of the cross-section. The analytical and computed strains ϵ_{xz} in the cross-section are plotted in figure 3(b). The shear strains are perfectly well computed by the enhanced beam element in this case.

3.2. Warping under transverse shear and torsion

Once the linear elastic behavior under transverse shear is validated, the response of the enhanced model under shear and torsion is investigated. The same cantilever beam is tested. A load $\mathrm{F} = -10\,\mathrm{kN}$ is applied at its free end in the z direction, along with a torsional moment $\mathrm{M} = 100\,\mathrm{Nm}$. The beam is discretized in 10 enhanced fiber beam elements. The cross-section mesh is

13

displayed in figure 4. Such a fine mesh would not be necessary for the result precision, since the cross-section elements are quadratic. This choice has been made to smooth the representation of the warped cross-section (figure 5(a)).
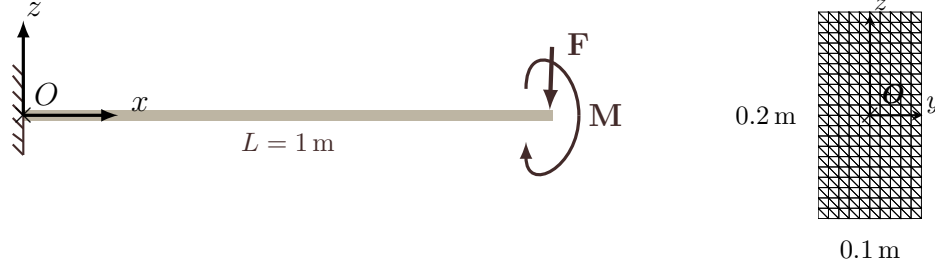

Figure 4: Case - study for the validation of the enhanced fiber beam element under shear and torsion: beam's geometry and loading; mesh of the cross-section.

The fiber element solution computed with **ATL4S** is compared to a 3D volumetric computation realized with the CAST3M [21] finite element software. The 3D beam is discretized using linear prismatic elements. Since the difference between the displacements computed by the beam formulation and the 3D finite element software is too tiny to be observable, an error indicator δ_{loc} is computed in equation 25. It quantifies the error between the warping displacements $U_{w,\text{beam}}$ obtained with the fiber beam element model and the 3D displacements $U_{w,3D}$. The values of δ_{loc} across the section are plotted in figure 5(b).

$$\delta_{loc} = \frac{\|U_{w,\text{beam}} - U_{w,3D}\|^2}{\max\left(U_{w,\text{beam}}\right)\max\left(U_{w,3D}\right)} \tag{25}$$

The error between the displacements obtained by the beam computation and the 3D computation reaches 5 % where the warping displacements are the greatest. The error does not exceed 1 % elsewhere in the cross section. It can be noted that the error increases close to the cross-section boundaries when the amplitude of the warping displacements increases. It is well-known that the Timoshenko's linear beam element does not give the exact solution for the plane-section displacements. In the enhanced element, the plane section displacements and the warping displacements are interdependent. The linear beam interpolation functions might not be accurate enough to
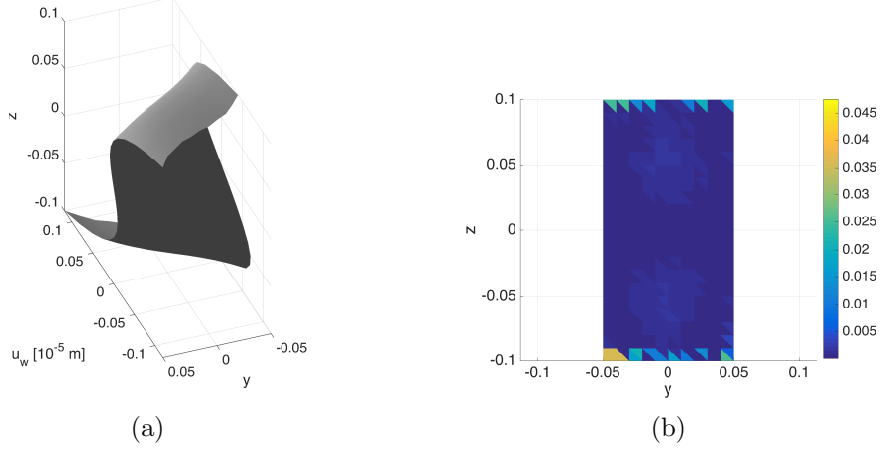
14

Figure 5: Results for the case-study of the cantilever beam under shear and torsion: 5(a): Warping displacements in the middle cross-section of the beam under shear and torsion. 5(b): Error δ_{loc} in the cross-section displacements between the enhanced fiber beam element model and the 3D discretization

give the exact warping solution. This can explain the difference between the beam-computed displacements and the 3D-computed displacements. A solution to further improve this result could be the use of a higher order beam element to implement the cross-section enhancement. Nevertheless, based on the presented results, the model and its implementation are considered as validated in the case of a linear elastic material behavior.

4. Numerical investigation of the nonlinear behavior using beams in torsion

The linear elastic behavior of the enhanced element has been validated in the previous part against an analytical solution and a 3D finite element solution. Now, the nonlinear behavior of the element is investigated. Monotonic torsion is modeled, with the aim of predicting experimental results.

4.1. Non linear material behavior

Concrete behavior is represented by a scalar damage model. The Mu model [22] is chosen because of its good representativeness for concrete shear behavior. The main equations of the model are summarized below. The constitutive law is given in equation (26). $\mathbf{\Lambda}_0$ is the initial stiffness tensor.

15

D_μ, given in equation (27), represents the activated part of damage. It depends on the two internal variables $Y_{\mu t}$ and $Y_{\mu c}$ (equation (28)), governing the yield surface's evolution in tension and compression. These variables are combined to compute the internal variable Y_μ according to the loading scenario. $Y_{\mu 0}$ denotes the initial value of Y_μ. A and B control the shape of the behavior curve after damage initiation.

The internal variables are defined from the extension strain $\varepsilon_{\mu t}$ and compressive strain $\varepsilon_{\mu c}$ in equation (28). The strains are computed from the two first strain tensor invariants I_ε and J_ε, as described in equation (29). $\varepsilon_{\mu t_0}$ and $\varepsilon_{\mu c_0}$ represent the damage thresholds. Two yield surfaces are associated to the internal variables, defined in equation (30).

$$\boldsymbol{\sigma} = (1 - D_\mu) \, \boldsymbol{\Lambda}_0 : \boldsymbol{\epsilon} \tag{26}$$

$$D_\mu = 1 - \frac{(1 - A) \, Y_{\mu 0}}{Y_\mu} - A \, \exp\left(-B \left(Y_\mu - Y_{\mu 0}\right)\right) \tag{27}$$

$$Y_{\mu t} = \max\left(\varepsilon_{\mu t_0}, \, \max_t \left(\varepsilon_{\mu t}\right)\right) \; ; \qquad Y_{\mu c} = \max\left(\varepsilon_{\mu c_0}, \, \max_t \left(\varepsilon_{\mu c}\right)\right) \tag{28}$$

$$\varepsilon_{\mu t} = \frac{I_\varepsilon}{2 \left(1 - 2\nu\right)} + \frac{\sqrt{J_\varepsilon}}{2 \left(1 + \nu\right)} \; ; \qquad \varepsilon_{\mu c} = \frac{I_\varepsilon}{5 \left(1 - 2\nu\right)} + \frac{6\sqrt{J_\varepsilon}}{5 \left(1 + \nu\right)} \tag{29}$$

$$f_{\mu t} = \varepsilon_{\mu t} - Y_{\mu t} \leq 0 \; ; \qquad f_{\mu c} = \varepsilon_{\mu c} - Y_{\mu c} \leq 0 \tag{30}$$

4.2. Beams subject to monotonic torsion

The experimental campaign of Chalioris and Karayannis [23] is chosen as a reference. This experimental campaign has already been used by the authors to validate a model with torsion-only induced warping [8]. The aim of the present study is first to check that the newly enhanced element can also predict the non-linear behavior of the plain concrete specimens in torsion, with a reasonable computational time. Then, the numerical behavior of the fully-implicit approach is investigated.

Several beams, with various cross-section shapes, have been tested in torsion. To highlight the effect of warping, five cross-section shapes have been selected for the present study. They are displayed in figure 6, with their respective mesh. One of the beams, namely the "L-shaped" cross-

section, is used for the material parameters calibration. The other beams are used to compare the behavior predicted by the model to the experimental results given in [23]. The behavior of the tested beams is simulated with both models without and with warping.

The concrete Young modulus has been estimated according to the experimental compressive strength and the European standard Eurocode 2 formula [24]. An arbitrary normal random field with a 5 % coefficient of variation has been included in the model for the Young modulus. The negative values have been truncated. This field is meant to coarsely represent the material spatial variability, which is very useful in applications with a homogeneous solicitation. This forces damage to initiate and develop in the weakest beam element, instead of a localization imposed by numerical round-off errors. Five different realization of the Young modulus random distribution have been computed for each cross-section shape.

The experimental material data are insufficient to determine the nonlinear material curve. This is why in the previous study [8], the material parameters describing the nonlinear material behavior have been calibrated, taking the experimental behavior of the "L-shaped" cross-section beam as a reference. The unknown parameters are the damage thresholds in compression and in tension, as well as the parameters A_c, B_c, and B_t which govern the shape of the damaged behavior curve. To calibrate these five unknown parameters, the aim is to simultaneously reproduce the material tensile and compressive strengths and the structural torque–twist curve for the L-shaped cross-section case. A genetic algorithm has been used to solve this multi-criteria optimization problem. A different set of parameters has been determined for both cases without and with warping, as the best fit for the L-shaped beam. More details on the calibration process, as well as on the resulting parameters, can be found in [8]. These two sets of parameters have been kept for the simulation of the behavior of the other cross-section shapes, without any fitting on the structural curve.

The beams are discretized using 4 displacement-based fiber beam elements. In pure torsion, the classical Timoshenko shape functions give the exact solution for the linear elastic case. There is no need to increase the number of elements. For the non-linear case, the choice of the element size governs the amount of dissipated energy. Since a softening material is modeled here, the solution will depend on the beam element size. The calibration of the material parameters takes this phenomenon into account The same size of beam elements is kept between the calibration case-study [8] and the other
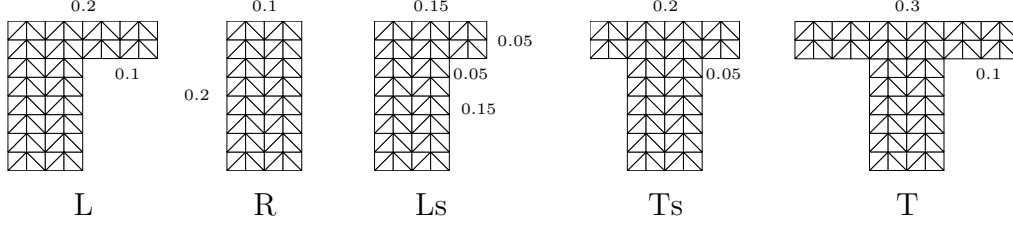
Figure 6: Dimensions [m] and mesh of the beams cross-sections

modeled beams. The torsion load is applied by enforcing the extreme rotations of the beams, up to 0.03 rad, in 50 steps. The predicted torque-twist curves with the fiber beam model without and with warping are presented in figure 7. Each curve is the mean torque-twist curve resulting from the 5 realizations of the Young modulus random field in the cross-sections. To quantify the ability of the numerical model to represent the experimental results, the relative difference between the numerical and experimental initial stiffness is computed. The results are given in table 1. The relative difference between the computed peak torque and the experimental peak torque is also computed, given in table 2.

Cross-section type	Ls	Ts	R	T
Without warping	160%	106%	126%	170%
With warping	35%	6%	38%	19%

Table 1: Relative difference between the numerical and experimental initial stiffness

Cross-section type	Ls	Ts	R	T
Without warping	21%	7%	15%	24%
With warping	16%	6%	27%	13%

Table 2: Relative difference between the numerical and experimental peak torque values, for both classical and enhanced models.

As shown in figure 7, the enhanced model predicts the experimental torque-twist behavior better than the plane cross-section model. By enforcing a plane cross-section, the classical fiber beam element model reduces
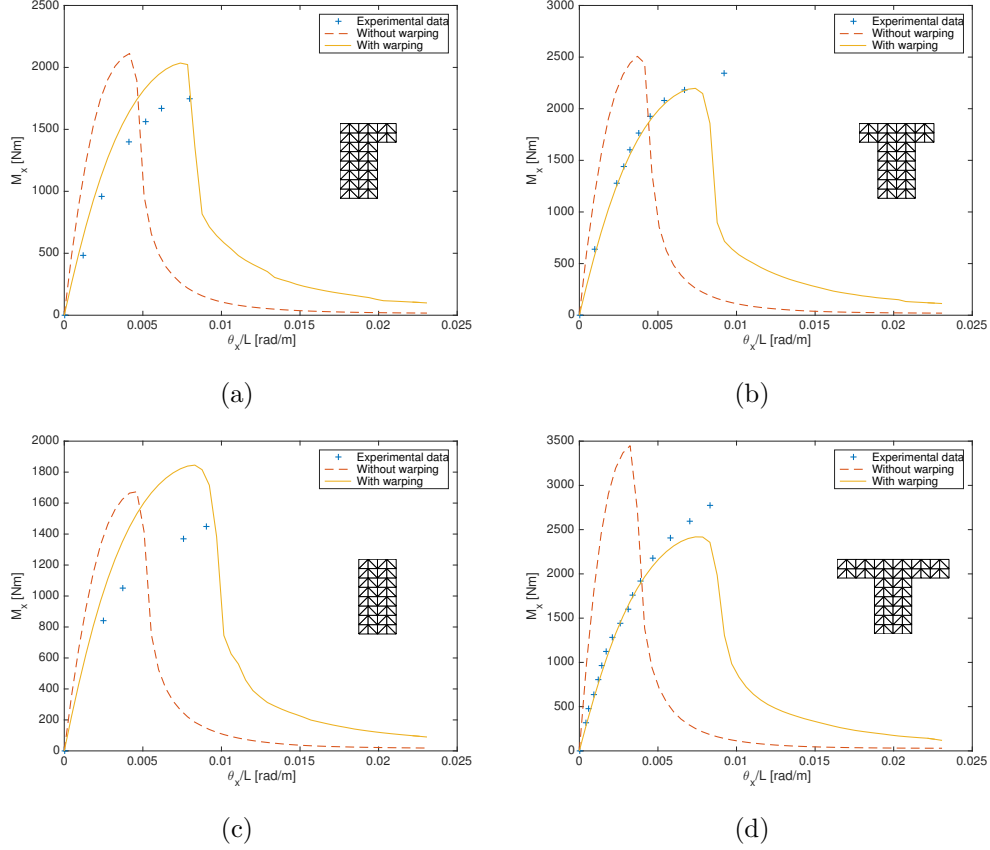
Figure 7: Comparison of the experimental and predicted torque-twist curves. 7(a) Ls cross-section; 7(b) Ts cross-section; 7(c) R cross-section; 7(d) T cross-section.

the freedom of the cross-section movement. This leads to a too stiff torque-twist curve in the linear range of the behavior. In average, the prediction of the initial stiffness is improved by 83 % when adding the warping degrees of freedom. This result is consistent with previously obtained conclusions on torsion-only warping models [7, 8]. The prediction of the peak torque is comparable for both numerical models, but the model without warping results in a more fragile behavior. The energy dissipated up to the peak is computed by numerical integration of the experimental and numerical torque-twist curves. The relative difference between the numerical and experimental energy is displayed in table 3. It shows that the prediction of the non-linear torque-twist

19

behavior is improved by 63% in average by including warping in the model. The experimental post-peak behavior is not available, due to the sudden failure of the plain concrete samples [23].

Cross-section type	Ls	Ts	R	T
Without warping	37%	60%	40%	50%
With warping	6%	28%	18%	20%

Table 3: Relative difference between the dissipated energy before failure, for both classical and enhanced models.

To illustrate the importance of modeling the local material behavior with good accuracy, damage maps of the beam cross-sections are displayed in figure 8. The value of damage is computed at the integration points of the cross-section, which directly correspond to the integration points of the quadratic triangles. After the peak, damage localizes in a single beam element. The damage maps of figure 8 correspond to the cross-section of this element, right after the torque-twist peak. It can be observed that the damage distribution is very different from the circular shape it would have in the case without warping [8, 18]. Accurate information on damage is indeed necessary to quantify the crack opening or to obtain the right deformation in rebars in case of reinforced concrete.
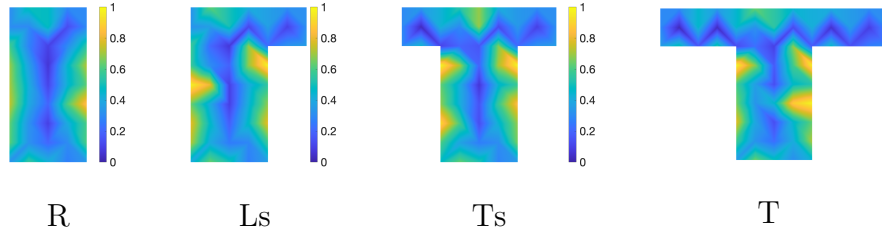

Figure 8: Damage maps of the cross-section where damage localizes right after the peak.

As already stated, damage localization induces a mesh dependency. This phenomenon is well-known for classical beam elements with a softening material, and is not specific to the enhanced element presented here. It is taken into account in this example through the calibration of the constitutive law on

Cross-section type	Ls	Ts	R	T
Without warping	906 s	994 s	703 s	1200 s
With warping	1490 s	2300s	1350 s	2550 s

Table 4: Mean computational time for each case study.

the "L-shaped" cross-section behavior and a mesh kept constant throughout all the simulations. To further enhance the model, regularization techniques can be used, based for example on Hillerborg's strategy [25, 26] or on non-local methods [27, 28]. Higher-order beam elements internally accounting for discontinuities could also be used [29], but the kinematic enhancement of such elements would require further developments.

Adding warping degrees of freedom to the fiber beam elements improves the prediction capacity of the nonlinear beam behavior. On the other hand, it slows down the computation of the solution. To investigate the effect of the enhancement on the computational time, the elapsed time for each case-study is displayed in table 4.

In average, the enhanced formulation is twice as computationally demanding as standard fiber beam elements. Nevertheless, the computation of the non-linear behavior of a beam only takes a few minutes on a conventional laptop. Thus, this drawback of the enhanced formulation will not prevent computations at the structural scale.

4.3. Influence of the size of load steps

To further investigate the nonlinear numerical behavior of the enhanced beam element, the influence of the load step size is studied. Several numerical tests are carried out on the beam with the rectangular cross-section presented in the previous paragraph. A rotation of 0.03 rad is applied, respectively in 25, 50, 100, and 200 steps. The resulting torque-twist curves are displayed in figure 9. This last case-study shows that there is no influence of the rotation step size on the material behavior. This result confirms that the formulation is fully implicit.

5. Nonlinear behavior of a reinforced concrete column subject to cyclic transverse loading

In the previous part, the importance of taking warping into account has been assessed by simulating the behavior of concrete beams in torsion. Nev-
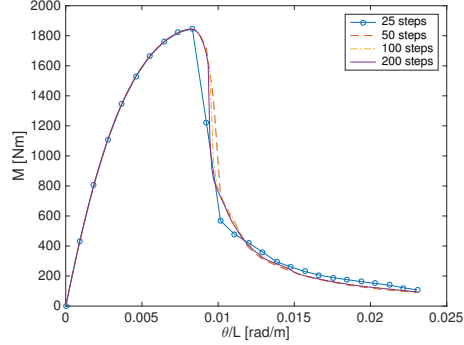
Figure 9: Results for the model with warping applied to the R-cross-section beam, with different rotation-step sizes.

ertheless, the ability of the model to account for reinforcement in concrete has not been demonstrated yet. Furthermore, for seismic applications, investigating the monotonic behavior is not enough. For these reasons, the case of columns subject to reverse cyclic bending is investigated here. The goal of this study is first to check that the proposed model is able to reproduce the cyclic experimental response of a reinforced concrete column in bending. Then, the effect of warping when the shear stress part increases is investigated.

5.1. Presentation of the case-study

The experimental campaign of [30, 31] has been chosen. Square reinforced concrete columns have been tested under a constant axial load and a reverse cyclic imposed top displacement. The specimen "C80B60N40" has been selected for the present study, as the specimen with the least high concrete strength, among the ones presented in [32]. This 2 meter-high column is represented in figure 10(a) with its square cross-section. The longitudinal reinforcement consists in 4 steel rebars of diameter 19.5 mm placed in the cross-section corners, and 4 steel rebars of diameter 16 mm in the middle of each edge. Stirrups ensure the lateral reinforcement and confine the central concrete part of the cross-section. A constant axial load of 2900 kN is imposed on the column.

The cross-section mesh is represented in figure 10(b). The concrete cross-section is discretized into 6-node quadratic triangles. The element size is given by the width of the cover zone, pictured in black in figure 10(b). It has
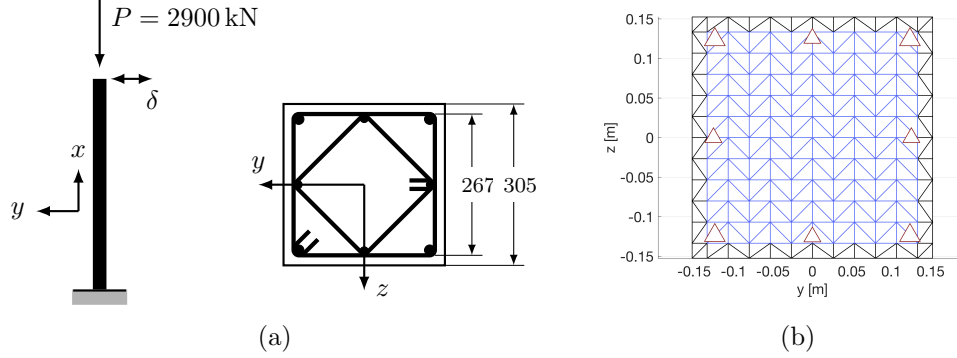
Figure 10: Representation of the tested column. 10(a) Column with its square cross-section. Dimensions of the section are given in mm. 10(b) Ccross-section discretization.

been chosen to discretize the confined concrete part of the cross-section with a similar element size, which explains the relatively high number of elements in the cross-section. The confined concrete part of the cross-section is represented by blue elements in figure 10(b). Each longitudinal rebar is modeled by one 6-node quadratic triangle. The warping degrees of freedom are the concrete cross-section nodes, but the deformations in the steel rebars are computed taking warping into account. Stirrups cannot be directly modeled in a fiber beam element approach. Their effect on the column's behavior can however be taken into account through the confined concrete constitutive law, as proposed by [32, 33].

Concrete is represented by the Mu model, described in section 4.1. In addition to its good representativeness of the concrete shear behavior, the Mu model takes into account the unilateral effect. It is thus relevant to represent the material behavior during a cyclic test. The input parameters of the model are the Young modulus and Poisson's ratio of concrete, the compression and tension stress thresholds y_{c0} and y_{t0}, and parameters that govern the post-peak constitutive behavior in compression and tension A_c, B_c, A_t, and B_t. The Young modulus E for concrete is calibrated on the linear elastic part of the experimental response of the column. The other material parameters are calibrated such that the material uniaxial compressive behavior reaches the peak strength and deformation given in [32]. The chosen material parameters are presented in table 5.

An elasto-plastic model with kinematic hardening is used for steel. The

23

Concrete	E	ν	y_c	y_t	A_c	B_c	A_t	B_t
Confined	28 GPa	0.2	-80 MPa	3 MPa	0.7	145	0.8	8000
Unconfined	28 GPa	0.2	-80 MPa	3 MPa	1	800	0.8	8000
Steel	E_s	ν_s	f_y	ϵ_{sh}	f_{su}	ϵ_{su}		
	210 GPa	0.3	500 MPa	0.0023	710 MPa	0.11		

Table 5: Summary of the concrete and steel model constitutive parameters

1D Menegotto-Pinto model [34] has proven its effectiveness in many applications [3, 22, 35]. Classical material parameters have been chosen for the present case-study, summarized in table 5. f_y denotes the yield strength, ϵ_{sh} the corresponding yield strain, f_{su} the ultimate strength and ϵ_{su} the corresponding ultimate strain.

Because of the concrete softening behavior and localization phenomena, the numerical response of the column is sensitive to the beam element size. This fact has also been evidenced by [33], who proposed a calibration of the element size based on the experimental results and the identification of an "equivalent plastic hinge" [33, 36]. Based on this approach, [33] suggested to use 5 elements of length 40 cm to model the tested column. This choice has been adopted in the present study.

5.2. Numerical results for the experimentally-tested column

The force-top displacement curve computed using the enhanced fiber beam element model is displayed in figure 11, along with the experimental results. It is important to note that neither the element length nor the material parameters have been adjusted according to the experimental response in the present study. Taking this fact into account, the experimental behavior is reasonably well reproduced. The maximum force is slightly overpredicted by the model. The loading and unloading pathes, as well as the dissipated energy are well computed.

The result displayed in figure 11 validates the ability of the model with warping to compute the flexural behavior of a concrete column, accounting for the longitudinal rebars. However, it does not indicate the effect of warping itself. Indeed, the computed column is slender enough not to activate shear failure mechanisms. The results of the models with and without warping are displayed in figure 12. There is very little difference between the two
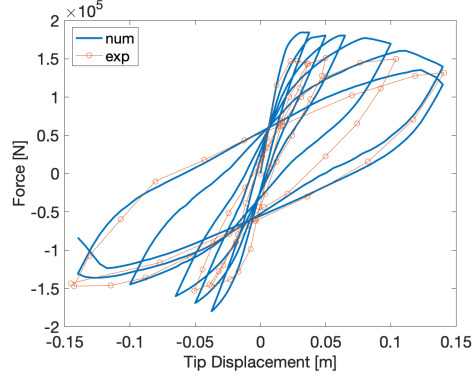
24

Figure 11: Prediction of the behavior of the column by the fiber beam element model with warping

diagrams, confirming that the effect of warping is negligible in this case. A shorter column is computed in section 5.3 to assess the effect of warping.
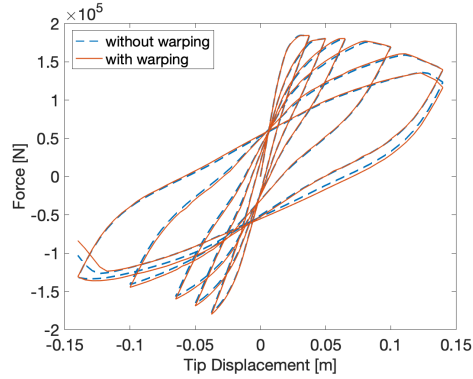

Figure 12: Numerical results for the column's behavior, using the model with warping or without warping.

5.3. Effect of warping on a shorter column

To observe the effect of warping, the column presented in the previous part is shortened to a length of 45 cm. This length corresponds to the limit at which shear becomes prevailing over bending. The material parameters of the 2-meter long column are kept, as well as the constant axial loading of

2900 kN. The transverse imposed displacement is adapted to the new column length. As mentioned in section 5.1, the numerical response depends on the beam element length. Since no reference data is available to calibrate the element length in this case, a length of 15 cm is chosen as a realistic length size for the energy dissipation due to the localized nonlinearities at the base beam element. The numerical results obtained with the models with and without warping are presented in figure 13.
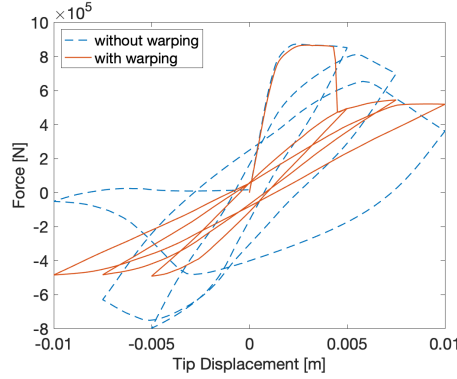

Figure 13: Numerical results for the short column's behavior, using the model with warping or without warping.

Although the curves of the models with and without warping are very close up to the first peak, the model with warping leads to a less ductile behavior. The rest of the cyclic behavior is strongly influenced by the addition of warping in the model. This post-peak difference is explained by the fact warping deformations increase when damage increases in the cross-section. Furthermore, the heterogeneity of the material properties between confined and unconfined concrete induces a variation of warping in the z-direction. Thus, the beam with warping encounters shear stresses in the xz-direction, contrarily to the beam without warping. This effect takes part in the more brittle failure of the beam when accounting for warping.

This study on a short column confirms that the shear warping enhancement is a necessary ingredient to compute the nonlinear behavior of a structural element, when dealing with great shear stresses. This is of major importance for short columns applications, such as parking lot columns for example, or partial infill frames.

26

6. Conclusion

To improve the shear response of the fiber beam element method, a new element is presented in this paper. Warping degrees of freedom are introduced in a Timoshenko displacement-based fiber beam element. Warping is allowed to vary both in the longitudinal and transverse directions of the beam. Added to the classical beam degrees of freedom, the warping degrees of freedom are computed at the nodes by satisfying a local beam equilibrium. Plane section displacement solutions are removed from the warping displacement solution space by an orthogonal projection of the warping shape functions. The warping shape function derivatives are computed accordingly, which is the novelty of the proposed approach compared to existing models. The multi-scale formulation, with a 2D finite element mesh of the cross-section, enables a fine representation of the material state variation in the cross-section. Another advantage associated with the FE approach of the cross-section discretization is its flexibility. It is possible to use fewer elements in the zones that remain linear elastic, and to refine the mesh in the severely damaged zones only. The local and global equilibrium equations are solved simultaneously, using a fully implicit time integration procedure. This enables the evolution of warping and material damage to interact in the nonlinear computation of concrete structural elements.

The deformations computed by the enhanced element reproduce exactly the analytical deformations for a rectangular beam with a linear-elastic behavior. This case-study is a first step in the validation of the enhanced element formulation and implementation. It enables to fully trust the linear elastic transverse shear results. The linear elastic warping displacements under coupled transverse shear and torsion are then successfully compared to the displacements obtained by a 3D finite element model. This result demonstrates the ability of the enhanced element to deal with multiaxial loadings. To investigate the non-linear behavior, a monotonic torsion case study and a cyclic transverse shear case study are presented. As regards torsion, experimentally tested beams made of plain concrete are simulated with both the classical and the enhanced fiber beam element method. From the calibration of the material constitutive law on a single cross-section shape, the proposed enhanced fiber beam element method predicts accurately the entire torsional response of plain concrete beams with various cross-sectional schemes (rectangular, L-shaped and T-shaped). It could be extended to simulate the behavior of steel fiber reinforced concrete beams by the imple-

mentation of proper constitutive laws of the composite material. The results confirm the necessity of including warping in the formulation, to obtain a physically meaningful torsional behavior.

The case of a reinforced concrete column subject to an axial load and to cyclic bending is eventually investigated, to address the tranvserse shear response. If the warping add-on is unnecessary for a slender column, this case-study demonstrates the ability of the model to deal with the reinforcement rebars and a cyclic loading. A numerical test on a shorter column shows the influence of warping on the response when shear stresses prevail.

The representation of the shear behavior of structural elements is greatly improved by the enhancement. However, additional warping degrees of freedom need to be solved for, which makes the model more computationally demanding. Nevertheless, the enhancement still enables computations at the structural scale.

References

[1] S. Grange, P. Kotronis, J. Mazars, Numerical modelling of the seismic behaviour of a 7-story building: NEES benchmark, Materials and Structures 42 (2008) 1433–1442. URL: http://www.springerlink.com/index/10.1617/s11527-008-9462-y. doi:10.1617/s11527-008-9462-y.

[2] P. Kotronis, J. Mazars, S. Grange, C. Giry, Simplified modeling strategies for non linear dynamic calculations of rc structural walls including soil-structure interaction, in: IASS-IACM, 2008.

[3] E. Spacone, S. El-Tawil, Nonlinear analysis of steel-concrete composite structures: State of the art, Journal of Structural Engineering 130 (2004) 159–168.

[4] J. Mazars, P. Kotronis, L. Davenne, A new modelling strategy for the behaviour of shear walls under dynamic loading, Earthquake engineering & structural dynamics 31 (2002) 937–954.

[5] F. J. Vecchio, M. P. Collins, The modified compression-field theory for reinforced concrete elements subjected to shear., ACI J. 83 (1986) 219–231.

[6] J.-F. Dubé, Modélisation multicouche des voiles en béton armé, Revue française de génie civil 1 (1997) 285–307.

[7] J. Mazars, P. Kotronis, F. Ragueneau, G. Casaux, Using multifiber beams to account for shear and torsion: Applications to concrete structural elements, Computer Methods in Applied Mechanics and Engineering 195 (2006) 7264–7281.

[8] S. Capdevielle, S. Grange, F. Dufour, C. Desprez, A multifiber beam model coupling torsional warping and damage for reinforced concrete structures, European Journal of Environmental and Civil Engineering 20 (2016) 914–935.

[9] J. M. Bairan, A. R. Mari, Coupled model for the non-linear analysis of anisotropic sections subjected to general 3d loading. part 1: Theoretical formulation, Computers & structures 84 (2006) 2254–2263.

[10] J. M. Bairan, A. R. Mari, Multiaxial-coupled analysis of rc cross-sections subjected to combined forces, Engineering structures 29 (2007) 1722–1738.

[11] J. Bairan Garcia, A. Mari Bernat, Shear-bending-torsion interaction in structural concrete members: a nonlinear coupled sectional approach, Archives of Computational Methods in Engineering 14 (2007) 249–278.

[12] S. Mohr, J. M. Bairán, A. R. Marí, A frame element model for the analysis of reinforced concrete structures under shear and bending, Engineering Structures 32 (2010) 3936–3954.

[13] M. Poliotti, J.-M. Bairán, B-spline sectional model for general 3d effects in reinforced concrete elements, Engineering Structures 207 (2020) 110200.

[14] V. Le Corvec, Nonlinear 3d frame element with multi-axial coupling under consideration of local effects, Ph.D. thesis, University of California, Berkeley, 2012.

[15] P. Di Re, D. Addessi, A. Paolone, Mixed beam formulation with cross-section warping for dynamic analysis of thin-walled structures, Thin-Walled Structures 141 (2019) 554–575.

[16] J. P. Almeida, A. A. Correia, R. Pinho, Force-based higher-order beam element with flexural-shear-torsional interaction in 3d frames. part ii: Applications, Engineering Structures 89 (2015) 218–235.

[17] C.-L. Lee, F. Filippou, Frame elements with mixed formulation for singular section response, International journal for numerical methods in engineering 78 (2009) 1320–1344.

[18] D. Addessi, P. Di Re, A 3d mixed frame element with multi-axial coupling for thin-walled structures with damage, Fracture and Structural Integrity (2014) 178–195.

[19] T. J. Hughes, The finite element method: linear static and dynamic finite element analysis, Prentiss-Hall, Englewood Cliffs, NJ (1987).

[20] S. Grange, Modèles multi-échelles et algorithmes pour les simulations dynamiques: application 'a la vulnérabilité sismique des structures, Habilitation à diriger des recherches, Université de Grenoble-Alpes, 2015.

[21] A. Millard, Castem 2000 User Manual, Technical Report Rapport CEA-LAMBS No 93/007, Commissariat Francais Energie Atomique, Saclay, France, 1993.

[22] J. Mazars, F. Hamon, S. Grange, A new 3d damage model for concrete under monotonic, cyclic and dynamic loadings, Materials and Structures (2014) 1–15.

[23] C. E. Chalioris, C. G. Karayannis, Effectiveness of the use of steel fibres on the torsional behaviour of flanged concrete beams, Cement and Concrete Composites 31 (2009) 331–341.

[24] B. EN, 1-1: 2004 eurocode 2: Design of concrete structures, General rules and rules for buildings (1992).

[25] A. Hillerborg, M. Modéer, P.-E. Petersson, Analysis of crack formation and crack growth in concrete by means of fracture mechanics and finite elements, Cement and concrete research 6 (1976) 773–781.

[26] J. Mazars, S. Grange, Simplified strategies based on damage mechanics for concrete under dynamic loading, Philosophical Transactions of the Royal Society A: Mathematical, Physical and Engineering Sciences 375 (2017) 20160170.

[27] G. Pijaudier-Cabot, Z. P. Bažant, Nonlocal damage theory, Journal of engineering mechanics 113 (1987) 1512–1533.

[28] C. Giry, F. Dufour, J. Mazars, Stress-based nonlocal damage model, International Journal of Solids and Structures 48 (2011) 3431–3443.

[29] I. Bitar, N. Benkemoun, P. Kotronis, S. Grange, A multifiber timoshenko beam with embedded discontinuities, Engineering Fracture Mechanics 214 (2019) 339–364.

[30] F. Légeron, P. Paultre, Behavior of high-strength concrete columns under cyclic flexure and constant axial load, Structural Journal 97 (2000) 591–601.

[31] P. Paultre, F. Légeron, D. Mongeau, Influence of concrete strength and transverse reinforcement yield strength on behavior of high-strength concrete columns, Structural Journal 98 (2001) 490–501.

[32] F. Légeron, P. Paultre, Uniaxial confinement model for normal-and high-strength concrete columns, Journal of Structural Engineering 129 (2003) 241–252.

[33] F. Légeron, P. Paultre, J. Mazars, Damage mechanics modeling of nonlinear seismic behavior of concrete structures, Journal of Structural Engineering 131 (2005) 946–955.

[34] M. Menegotto, P. Pinto, Method of analysis for cyclically loaded reinforced concrete plane frames including changes in geometry and non-elastic behavior of elements under combined normal force and bending, in: IABSE Symposium on the Resistance and Ultimate Deformability of Structures Acted on by Well-Defined Repeated Loads, Lisbon, 1973.

[35] S. Mohr, Nonlinear static and dynamic model for the analysis of reinforced concrete frames under high shear forces, Ph.D. thesis, Universitat Politècnica de Catalunya, 2011.

[36] M. N. Priestley, F. Seible, G. M. Calvi, Seismic design and retrofit of bridges, John Wiley & Sons, 1996.